A semi-empirical framework for assessing the impact of biofouling on ship powering in tropical waters

Ocean Engineering 357 (2026) 125590

Contents lists available at ScienceDirect

Ocean Engineering

journal homepage: www.elsevier.com/locate/oceaneng

Research paper

A semi-empirical framework for assessing the impact of biofouling on ship powering in tropical waters

Youngrong Kim [a,*], Shukui Liu [b], Maria Lagerström [c], Lena Granhag [c], Erik Ytreberg [c,d]

[a] School of Civil and Environmental Engineering, Nanyang Technological University, Singapore, 636921
[b] School of Mechanical and Aerospace Engineering, Nanyang Technological University, Singapore, 639798
[c] Department of Mechanics and Maritime Sciences, Chalmers University of Technology, SE 412 96, Gothenburg, Sweden
[d] IVL Swedish Environmental Research Institute, SE 400 14, Gothenburg, Sweden

ARTICLE INFO

Keywords:
Biofouling
Antifouling coatings
Added resistance prediction
Ship powering performance
Voyage simulation
Tropical marine environment

ABSTRACT

One of the factors that hinders vessel operational efficiency is hull fouling, especially in tropical waters where biofouling is prevalent and high water temperatures persist year-round. Accurately predicting and managing the impact of biofouling on ship performance is critical, but there is a lack of research on methodologies that can easily provide the impact of hull fouling growth and maintenance on ship performance under various conditions in tropical regions. This study develops a novel semi-empirical framework for predicting performance changes due to hull fouling of ships operating in tropical waters. This framework incorporates modules that predict hull roughness changes, which are based on field testing of marine coatings in tropical waters, as well as comprehensive ship resistance and propulsion performance, and the impact of maintenance. Through simulations of various operational and management scenarios, the proposed framework demonstrated its capability to quantitatively predict hull roughness changes, associated energy penalty, and resulting carbon intensity indicator and to evaluate the long-term effectiveness of different strategies. Importantly, the proposed framework is applied within a scenario-based analysis to explore potential impacts of hull biofouling on ship powering and CII performance in tropical waters, rather than serving as a fully validated predictive model. In conclusion, the developed framework is expected to serve as a practical decision-support tool for ship operators in selecting optimal antifouling coatings and establishing effective hull maintenance plans, thereby enhancing energy efficiency and reducing emissions.

1. Introduction

International shipping is facing the challenge of improving operational efficiency due to increasing greenhouse gas (GHG) emissions regulations (Bouman et al., 2017; IMO, 2023; IPCC, 2022). One of the key factors impeding this efficiency is so-called biofouling, where marine organisms attach to the hull surface. By increasing the roughness of the hull surface due to biofouling colonies, it increases more frictional drag on the ship (Demirel et al., 2017; Townsin, 2003), and it is reported to contribute to approximately 10% of GHG emissions from worldwide shipping (Farkas et al., 2021; Kim et al., 2023).

This problem is particularly acute in tropical marine environments. The region's high water temperatures, abundant nutrients, and strong year-round sunlight create ideal conditions for rapid and severe biofouling growth (Madin et al., 2009; Satheesh et al., 2016; Thomas et al., 2021). Since many of the world's busiest shipping routes, like the Straits of Malacca and the Port of Singapore, are in tropical waters (UN, 2021), managing biofouling in these areas is a pressing issue for ship operations and the environment.

To combat this, the maritime industry primarily relies on specialized antifouling coatings and regular hull maintenance, such as in-water cleaning. The effectiveness of these antifouling systems is crucial, but predicting their long-term efficacy in diverse operational contexts remains a significant challenge. This uncertainty impacts not only performance maintenance but also wider operational strategies like optimal route planning, which makes the accurate prediction and management of biofouling essential for sustainable ship operations (Kytariolou and Themelis, 2023).

Several methods have been attempted to quantitatively estimate the impact of biofouling on ship propulsion performance. While valuable for

* Corresponding author.
E-mail address: youngrong.kim@ntu.edu.sg (Y. Kim).

https://doi.org/10.1016/j.oceaneng.2026.125590
Received 10 July 2025; Received in revised form 20 March 2026; Accepted 11 April 2026
Available online 17 April 2026

detailed analysis, methods like Computational Fluid Dynamics (CFD) (Demirel et al., 2017; Martić et al., 2021; Song et al., 2019) and traditional water tank model tests (Song et al., 2021; Uzun et al., 2017, 2020) face practical limitations for broad, long-term assessments. CFD can offer precise flow-field information using fully non-linear methods and can overcome certain limits of theoretical approaches like boundary layer analysis (Demirel et al., 2017; Song et al., 2019). However, its significant computational expense makes large-scale parametric studies for various operational scenarios prohibitive (Song et al., 2021). Similarly, model testing provides direct physical measurements but involves costly set-up systems and facility time (Atlar et al., 2018). Recently, data-driven models utilizing ship operational data, such as artificial intelligence and machine learning, have been actively studied, but they are limited by the difficulty of physical interpretation of the results and the difficulty of obtaining good quality long-term data covering a wide range of conditions (Bakka et al., 2022; Guo et al., 2023; Laurie et al., 2021; Shaw and Lin, 2021).

Considering the trade-offs of these methodologies, semi-empirical models that combine hydrodynamic principles with empirical data present an efficient and practical alternative. These models often leverage robust and economical techniques, such as the boundary layer similarity law scaling proposed by Granville (1958), to estimate ship's frictional resistance coefficient (Kim et al., 2025; Liu et al., 2023; Oliveira et al., 2022; Ozyurt et al., 2023; Thomas et al., 2021; Uzun et al., 2019). This approach maintains physical interpretability and is computationally efficient, allowing for the long-term, dynamic voyage simulations that are impractical with CFD or physical model tests alone.

However, many existing semi-empirical models rely on simplified assumptions, such as assigning pre-defined or static hull roughness values to represent different fouling conditions, rather than modeling the dynamic growth over time (Kytariolou and Themelis, 2023; Liu et al., 2023; Thomas et al., 2021). While some time-dependent fouling growth models have been proposed (Oliveira et al., 2022; Ozyurt et al., 2023; Uzun et al., 2019), there remains a notable research gap in comprehensively predicting ship performance changes under the unique environmental conditions of tropical waters, especially considering the effects of different hull maintenance strategies. This lack of tailored prediction models is a practical constraint to establishing optimal maintenance plans for vessels operating in these regions.

To overcome these limitations, this study proposes a novel semi-empirical ship performance prediction framework that considers the impact of hull fouling specifically in tropical waters. Specifically, the present study adopts and extends the fouling-growth modelling approach proposed by Oliveira et al. (2022), applying it to compiled tropical biofouling datasets and exploring its implications for ship powering and carbon intensity indicators. The developed model aims to enable long-term dynamic simulation of ship performance due to hull fouling under different operational and environmental conditions with interpretability and computational efficiency, which can predict key indicators such as fuel consumption and environmental performance indicators such as the carbon intensity indicator. Therefore, it ultimately supports science-based decision-making for energy efficiency optimization and sustainable operation of ships operating in tropical waters by providing quantitative comparisons of different coating systems, operational profiles, and maintenance interventions.

2. Modeling approach

2.1. Overall framework

In this study, a semi-empirical model is developed to predict the time-dependent impact of hull fouling on ship performance in tropical waters. Fig. 1 shows the overall framework of the model, which is designed as a modular structure with key input data, three core computational modules, and a dynamic feedback loop to derive the final output. This structure enables the simulation of long-term changes in ship performance due to hull roughness changes and maintenance activities. The model framework consists of the following main modules.

Module 1: Fouling growth & Hull roughness estimation module estimates the change in equivalent sand roughness over time based on inputs (ship operational profile, antifouling systems, tropical waters field data, etc). This module initializes hull roughness and simulates fouling regrowth when hull maintenance activities occur.

Module 2: Ship's total resistance estimation module uses the hull roughness calculated in Module 1 and the surrounding environmental conditions (wind, waves, etc.) to calculate the total resistance at that point in time (see Section 2.3). The total ship resistance is composed of the sum of calm water resistance, added resistance due to hull fouling, and added resistance due to external environments, and utilizes a semi-empirical formula based on widely accepted literature and standards.

Module 3: Ship's power estimation module estimates the main engine brake power required to overcome the total drag calculated in Module 2 and maintain the target speed, taking into account the overall propulsion efficiency (see Section 2.4). If the calculated power or related

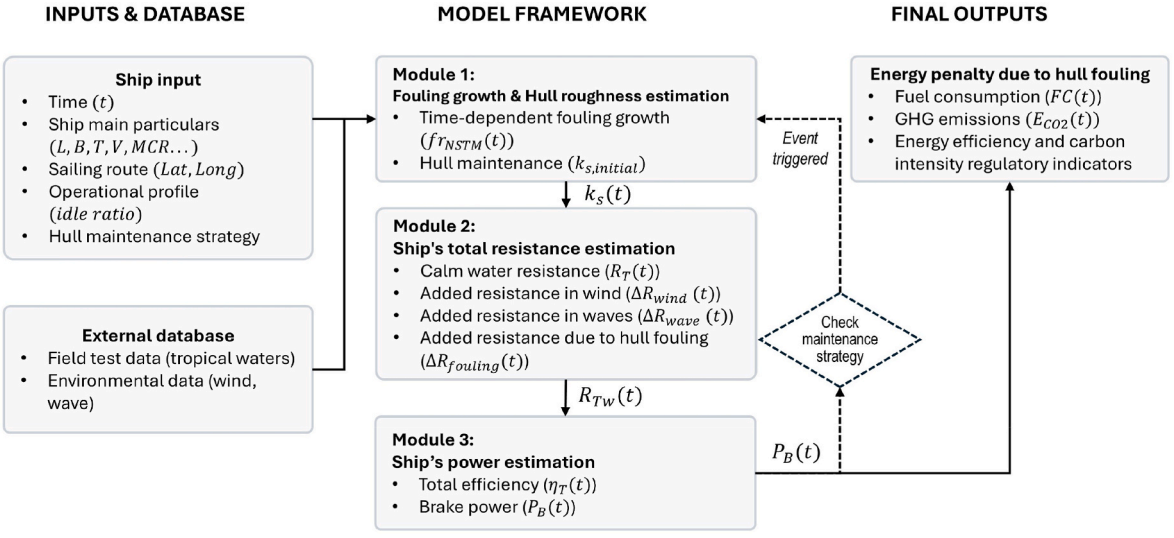

Fig. 1. Overall model framework diagram for time-dependent semi-empirical method for predicting ship power performance considering the impact of biofouling in tropical waters.

performance metric exceeds a set threshold, a 'cleaning event' is triggered, activating a dynamic feedback loop that updates the hull roughness value from Module 1. Finally, the model calculates hourly fuel consumption and GHG emissions of the operating ship, which determine environmental indicators such as the carbon intensity indicator. The details of each module are described in subsequent sections.

2.2. Hull roughness & fouling growth module

This module predicts the change in hull roughness as a function of time due to the accumulation of biofouling on the hull of a ship operating in tropical waters. The main output of this module is the equivalent sand-grain roughness (k_s), which is used as an input variable for the subsequent resistance calculation module (Section 2.3) to estimate the additional frictional resistance due to fouling ($\Delta R_{fouling}$).

2.2.1. Field test data

To develop a hull fouling growth model applicable to tropical waters, this study compiled data from existing research on field tests. The primary inclusion criteria for the data were that the studies involved static immersion of coated panels in tropical marine locations and reported the progression of bio-attachment over time. Most of the collected data have in common the exposure of the test panels to realistic seawater environments, and the main information of each test is summarized in Table 1.

For the purpose of this analysis, the coatings from the compiled studies were categorized based on their functional mechanisms. The primary antifouling systems analyzed fall into two main groups: biocidal antifouling coatings (AFC) and foul-release coatings (FRC). AFCs, often referred to as conventional systems, function through the controlled release of biocides to deter the settlement and growth of marine organisms. This category includes various technologies, such as Self-Polishing Copolymers (SPC), which are designed to provide a consistently smooth and active surface. In contrast, FRCs are typically biocide-free systems that feature a smooth, low-surface-energy, non-stick surface, often silicone-based. This characteristic does not prevent organism settlement but instead reduces adhesion strength, allowing fouling to be released or washed away by the water flow generated by the ship's movement.

In addition to these protective topcoats, data for anticorrosive coatings (AC) were included to serve as a scientific benchmark. Although ACs are used in practice as a primer for corrosion protection and not as a final topcoat, here they were used to represent a control or baseline condition. This effectively models a hull surface that has lost its antifouling properties, such as due to mechanical damage, coating degradation, or exceeding its service life. Thus, it allows for a quantitative assessment of the maximum potential impact of biofouling.

As shown in Table 1, each study exhibits variations in experimental conditions, including the specific geographical location of the test site, seawater characteristics, panel installation setup, and exposure time. While potential regional variations were observed in the data, the available studies utilized differing experimental protocols. This heterogeneity across the compiled dataset makes it statistically challenging to reliably decouple potential location-specific fouling pressure from other confounding experimental variables. Therefore, to maintain robustness with the available data, this study groups the data to model the generalized fouling growth trend for tropical waters as a whole, acknowledging this generalization as a limitation. Consequently, the potential influence of experimental condition variability on fouling growth was quantitatively reflected in the subsequent modeling process through confidence intervals (CIs).

2.2.2. Time-dependent fouling growth model

The field datasets collected from various sources in Section 2.2.1 describe fouling conditions in slightly different ways. In order to compare and analyze these disparate data on a consistent basis and to normalize the fouling observations reported in each study to a common scale, this study adopts the fouling scale defined by the US Naval Ships' Technical Manual (NSTM) (US Navy, 2006). The NSTM fouling scale (FR_{NSTM}) is categorized into 10 subdivided scales ranging from 0 to 100 based on the severity of the biofouling species, with increasing values indicating that the surface is covered with a combination of rougher and harder fouling. The average NSTM fouling rating ($\overline{FR_{NSTM}}$) of the panel surface is calculated from Eq. (1), taking into account the type of fouling and the area covered. Considering the typical operation and cleaning cycles of the vessel and the limited amount of data, the data up to one year after the start of exposure were extracted and utilized for the development of the time-dependent fouling growth model in the study.

$$\overline{FR_{NSTM}} = \sum_{i=1}^{N} \frac{FR_{NSTM,i} \times \%cover_i}{100} \tag{1}$$

where $\overline{FR_{NSTM}}$ is the average NSTM fouling rating of the panel surface, $FR_{NSTM,i}$ is the NSTM fouling rating of the i-th fouling type, $\%cover_i$ is the percentage of area covered by the i-th fouling type, and N is the total number of different fouling types observed.

To predict average coating-specific fouling development over time in tropical waters, the Gaussian formulation in Eq. (2) is retained as a

Table 1
Summary of compiled field test data conducted in tropical environments used for biofouling growth modelling in this study.

Source	Test site (Region)	Coordinates	Installation details	Exposure duration	Environmental conditions	Coating types
Holm et al. (2008)	Singapore Yacht Club (Singapore)	1°17′40.0″N 103°45′37.6″E	Installed on the raft (0.5m depth)	2 years (2005/12-2007/11)	Salinity 28-33 ppt; Temp 27-30 °C	AC (Intergard); AFC (BRA 640); FRC (Intersleek 425)
Nuraini et al. (2016)	Muara Baru port (Jakarta, Indonesia)	6°06′S 106°48′E (Coordinates of Muara Baru port)	Submerged panel (0-3m depth)	3 months	Salinity 28.15 ppt; Temp 30.15-30.45 °C	2 x AC (commercial); 2 x AFC (commercial)
Kardela (2019)	Changi Sailing Club (Singapore)	1°23′35.4″N 103°58′43.5″E	Installed on the raft (0.5m depth)	2 months (2017/07-2017/09)	Salinity 31.53 ppt; Temp 29.54 °C (Yearly average estimated from ECMWF reanalysis data)	FRC (Intersleek 1100SR)
Kolle et al. (2022)	Singapore Yacht Club (Singapore)	1°17′40.0″N 103°45′37.0″E	Not specified	2 years (2015/06-2017/05)	Salinity 20-30 ppt; Temp 27-31 °C	PMDS control; FRC (Intersleek 700)
Priyotomo et al. (2022)	Madura Strait (Indonesia)	7°10′56.5″S 112°46′50.7″E	Installed on the bridge pile	3 months	Salinity 28.5-28.7 ppt; Temp 29.05-32.25 °C	2 x AC (commercial); 2 x AFC (commercial SPC)
Prifiharni et al. (2024)	Gulf of Benoa (Indonesia)	8°46′S 115°12′E (Coordinates of Mandara highway)	Installed on the bridge pile (0-3m depth)	1 year (2015/10-2016/09)	Salinity 29.4-35 ppt; Temp 29-31.5 °C	2 x AC (commercial); 2 x AFC (commercial)
Priyotomo et al. (2024)	Muara Baru port (Jakarta, Indonesia)	6°05′46.0″S 106°48′01.0″E	Installed on the pile (0-3m depth)	1 year	Salinity 28.1-31.1 ppt; Temp 29.75-30.9 °C	2 x AC (commercial); 2 x AFC (commercial)

parsimonious empirical functional form. The Gaussian function has been used in previous studies to model fouling growth as it can effectively represent the initial accumulation phase of the S-shaped growth curve commonly observed in biological growth, i.e., the onset of progressive fouling and changes in growth rate (Oliveira et al., 2022; Uzun et al., 2019). In the present study, however, the coefficients were re-estimated separately for the compiled tropical AC, AFC, and FRC datasets described in Section 2.2.1. Therefore, no fitted coefficients were transferred directly from Oliveira et al. (2022). Given the limited, unevenly sampled, and heterogeneous nature of the available tropical datasets, these functions are intended to represent generalized coating-specific fouling-growth trends over the considered exposure period for scenario analysis.

$$\widehat{FR_{NSTM}}(t) = a \times e^{-\left(\frac{t-b}{c}\right)^2} \tag{2}$$

where $\widehat{FR_{NSTM}}(t)$ is the predicted NSTM fouling rating at cumulative exposure time t [days]. The coefficient a is fixed at 100, the theoretical maximum value of FR_{NSTM}, and b and c are the model coefficients that determine the location and shape of the fouling growth curve. To obtain the model coefficients b and c, a weighted non-linear least squares method was applied to minimize the sum of the squared errors between the observed data ($\overline{FR_{NSTM}}$) and the predicted data ($\widehat{FR_{NSTM}}$). The weight given to each data point was set to take into account the standard error of the corresponding observed data, which gives more weight to data with smaller standard errors.

Finally, the equivalent sand-grain roughness due to hull fouling ($k_{s,fouling}$) is obtained by converting the predicted NSTM fouling rating ($\widehat{FR_{NSTM}}$) values using Eq. (3). This equation is an exponential function adopted from Oliveira et al. (2022). This correlation was developed by fitting the experimental data and $k_{s,fouling}$ estimates for various fouling conditions originally presented by Schultz (2007).

$$k_{s,fouling}(t) = 46.927 \times e^{0.056614 \times \widehat{FR_{NSTM}}(t)} \tag{3}$$

where, $k_{s,fouling}(t)$ is the equivalent sand-grain roughness [μm] due to the hull fouling at time t, and $\widehat{FR_{NSTM}}(t)$ is the predicted NSTM fouling rating at time t.

Fig. 2 visually presents this relationship, which plots the original data ranges from Schultz (2007) against the fitted curve (Eq. (3)). While discrete $k_{s,fouling}$ estimates for specific fouling types exist, the use of a continuous function is more practical for a semi-empirical framework, which models the progressive growth of fouling over time. This $k_{s,fouling}(t)$ is subsequently used as an input in calculating the increased frictional resistance of the ship due to hull fouling.

2.2.3. Hull maintenance model

As established, managing the performance degradation caused by biofouling requires crucial maintenance operations. These can be periodic or condition-based, and include in-water hull cleaning (IWHC), propeller cleaning, dry-docking, and re-coating of the hull. In this model, it is assumed that after a specific maintenance operation, the hull surface roughness returns to a certain predefined initial value depending on the effect of the activity. Representative initial hull roughness values, expressed as equivalent sand-grain roughness after various maintenance activities, were collected from existing literature (Atlar et al., 2018; Leer-Andersen, 2018; Schultz, 2007; Yeginbayeva and Atlar, 2018) and publicly available friction resistance databases, as summarized by Oliveira et al. (2022) in Table 2, and they were used in this study.

Table 2
Initial hull roughness after performing specific hull maintenance activities adapted from Oliveira et al. (2022).

Hull maintenance activity	Initial hull roughness in $k_{s,init}$ [μm] (Lower/Average/Upper bound)
Full sandblasting & new foul-release coating application	0/15/30
Full sandblasting & new antifouling and inert coating application	30/40/60
Touch-up coating: foul-release coating	35/40/45
Touch-up coating: polishing antifouling and inert coating	30/65/150
Proactive IWHC, negligible coating wear	Same as out-docking condition (assumed no coating deterioration)
Proactive IWHC, moderate coating wear	50/80/150 (assumed best cleaning practices)
Reactive IWHC, high coating wear	70/150/300 (assumed light cleaning or imperfect cleaning)

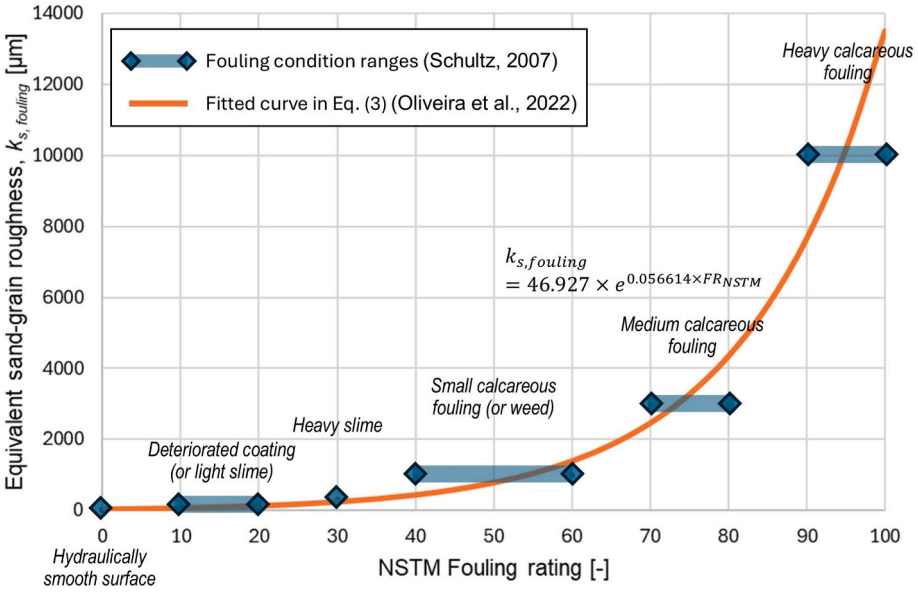

Fig. 2. Correlation between NSTM Fouling rating (FR_{NSTM}) and equivalent sand-grain roughness (k_s). The data points with shaded horizontal bars represent the estimated k_s values and associated FR_{NSTM} ranges described in Schultz (2007). The solid line is the exponential function fitted by Oliveira et al. (2022) with $R^2 = 0.96$.

After a maintenance activity, the hull surface roughness is reset to a specific initial value. This study models the total equivalent sand roughness at a time t' elapsed since the last maintenance ($k_{s,total}(t')$) by assuming that the roughness from new fouling growth ($k_{s,fouling}(t')$) superimposes on the initial post-maintenance hull roughness ($k_{s,init}$). This relationship is expressed in Eq. (4):

$$k_{s,total}(t') = k_{s,init} + k_{s,fouling}(t') \tag{4}$$

where $k_{s,total}(t')$ is the total equivalent sand-grain roughness [μm] of the hull at elapsed time t' after the maintenance event, and $k_{s,init}$ is the initial equivalent sand-grain roughness [μm] immediately following maintenance (values are given in Table 2), which represents the baseline roughness of the hull surface. The average value from Table 2 is used for $k_{s,init}$ in mean prediction simulations, while the range (Lower/Upper bounds) is considered in uncertainty assessments. $k_{s,fouling}(t')$ is the equivalent sand-grain roughness [μm] contributed by new biofouling that has accumulated over the elapsed time t'. This value is calculated using the time-dependent fouling growth model described by Eq. (2) and Eq. (3), where the time variable is reset to zero at the moment of maintenance ($t' = 0$).

The modeling of hull maintenance within this framework involves simplifications appropriate for its intended scope as a foundational tool. The framework incorporates various hull maintenance activities by resetting the hull roughness to an initial value after an event. Recognizing that actual post-maintenance roughness can vary depending on the cleaning method and intensity (Lin et al., 2023; Oliveira and Granhag, 2020), this mechanism allows users to reflect ship-specific activities by adjusting the $k_{s,init}$ value, using the representative values and ranges provided in Table 2 as a guideline or employing specific data if available. Following this reset, the linear addition of the roughness values from new fouling growth (Eq. (4)) is used. While this linear addition is a simplified representation of complex physical phenomena, such as interactions between residual topography and new fouling, it serves as a pragmatic method for estimating hull roughness changes over time when detailed topographical data is difficult to obtain.

2.3. Ship resistance estimation module

This module calculates the total resistance experienced by the ship in a given sea state, given the ship's operational profile at a given point in time. The total resistance (R_{Tw}) is given by Eq. (5), which consists of the calm water resistance (R_T), added resistance due to surrounding environmental factors such as added resistance in wind (ΔR_{wind}) and waves (ΔR_{wave}), and added resistance due to hull biofouling ($\Delta R_{fouling}$).

$$R_{Tw} = R_T + \Delta R_{wind} + \Delta R_{wave} + \Delta R_{fouling} \tag{5}$$

In this study, in line with the semi-empirical approach of the overall framework, the methods described in the procedures and guidelines recommended by the International Towing Tank Conference (ITTC) (ITTC, 2021, 2022) have been selected to estimate each of the above resistance components. These estimation methods can be replaced as needed when more detailed and accurate ship-specific information is available and other sophisticated methodologies such as CFD and model tests are utilized.

2.3.1. Calm water resistance

The resistance in calm water (R_T) is the resistance a vessel experiences when sailing on calm water, which is estimated in this study using the Holtrop-Mennen method (Holtrop, 1984; Holtrop and Mennen, 1982), a widely used semi-empirical method for a range of ship types, sizes, and Froude numbers. This method provides relatively satisfactory resistance estimates based on the vessel's main dimensions and ship form coefficients and is particularly useful in the early design phase or for performance analysis when detailed ship form information is lacking. The calm water resistance, according to the Holtrop-Mennen method, is calculated as the sum of several resistance components, as shown in Eq. (6).

$$R_T = R_F(1 + k_1) + R_{APP} + R_W + R_B + R_{TR} + R_A \tag{6}$$

where R_F is the frictional resistance, calculated using the frictional resistance coefficient based on the ITTC 1957 model-ship correlation line. $(1 + k_1)$ is the form factor, which accounts for the effect of the hull form on viscous resistance, R_{APP} is the appendage resistance, R_W is the wave-making and wave-breaking resistance, R_B is the additional pressure resistance of the bulbous bow near the surface, R_{TR} is the transom stern resistance, and R_A is the model-ship correlation allowance. The specific empirical formulas and coefficients required for calculating each of these resistance components follow those detailed in the original papers by Holtrop and Mennen (1982) and Holtrop (1984).

2.3.2. Added resistance in wind

The added resistance due to wind (ΔR_{wind}) refers to the extra resistance a ship encounters from wind effects while it is moving, and this resistance varies based on the ship's superstructure geometry, relative wind speed, and relative wind direction. In this study, it is calculated by subtracting the air resistance caused by the ship's own speed in stationary air from the total air resistance experienced by the ship as it moves forward with the wind following the procedure recommended by ITTC (2022) as shown in Eq. (7).

$$\Delta R_{wind} = \frac{1}{2}\rho_a A_V C_{DA}(\beta_{WRref}) {V_{WRref}}^2 - \frac{1}{2}\rho_a A_V C_{DA}(0) {V_{ref}}^2 \tag{7}$$

where ρ_a is the air density, A_V is the maximum transverse projected area exposed to the wind, and C_{DA} is the wind force coefficient, which is typically obtained from wind tunnel experiments. In this study, the wind force coefficient of the ship is estimated using Blendermann (1994) and Fujiwara (2006). β_{WRref} is the apparent wind angle, with the bow equal to zero. V_{WRref} is the apparent wind speed, and V_{ref} is the ship speed. The apparent wind angle and speed are calculated by considering the true wind speed and direction extracted based on the ship's actual location and the ship's heading and speed.

2.3.3. Added resistance in waves

The added resistance in waves is the additional resistance experienced when a ship is sailing through waves, caused by factors such as ship motions and wave reflection. It can account for a significant portion of the ship's total resistance, particularly in adverse weather conditions. In this study, added resistance in waves is estimated using the SNNM method, which was proposed by Liu and Papanikolaou (2020) and validated by Wang et al. (2021). This method is included in ITTC's recommended procedures (ITTC, 2022) for sea trials and offers the advantage of reasonably predicting added resistance in waves at arbitrary encounter angles quickly by using only the limited hull geometry information.

The mean added resistance in irregular sea states can be expressed in the form of Eq. (8):

$$\Delta R_{wave} = 2\int_0^{2\pi}\int_0^{\infty} \frac{R_{AW}(\omega, \alpha, V)}{{\zeta_a}^2} S_\zeta(\omega) G(\alpha) d\omega d\alpha \tag{8}$$

where ω is the wave angular frequency [rad/s], α is the wave encounter angle relative to the ship [degrees], and $R_{AW}(\omega, \alpha, V)/{\zeta_a}^2$ is the added resistance transfer function in regular waves, which can be calculated using the semi-empirical SNNM method. $S_\zeta(\omega)$ is the wave spectrum, for which standard models such as the JONSWAP or Pierson-Moskowitz spectrum, characterized by significant wave height (H_s) and peak period (T_p), can be used as appropriate for the conditions. $G(\alpha)$ is the wave directional spreading function, which can be determined with

reference to ITTC (2022) guidelines. The required wave input parameters are obtained from environmental data along the ship's route.

2.3.4. Added resistance due to hull roughness increase

Biofouling on the hull surface increases its roughness, which in turn causes an increase in the ship's frictional resistance. To quantify this effect, this study estimates the added resistance from biofouling ($\Delta R_{fouling}$) using Granville's (1958) similarity law scaling procedure. The selection of this indirect method is grounded in its established robustness, cost-effectiveness, and practicality for a semi-empirical framework. Compared to direct boundary layer measurements or full CFD simulations, Granville's scaling is simpler and more convenient, requiring less investment while demonstrating good agreement with both full-scale trial data and CFD studies (Demirel et al., 2017; Schultz, 2007; Song et al., 2019). Furthermore, its capacity to predict roughness-induced effects across various ship speeds and lengths makes it highly suitable for the scenario-based analysis central to this research.

Nevertheless, the inherent limitations of this methodology are acknowledged. As a boundary layer analysis conceived for an equivalent flat plate, Granville's method primarily predicts the change in frictional resistance. Consequently, this approach, relying on an averaged k_s input derived from complex fouling morphologies with Granville's scaling, does not fully capture other hydrodynamic effects such as the additional form drag from hard fouling, the influence of roughness on viscous pressure resistance, or interactions with the 3D hull form (Song et al., 2019). This limitation is considered acceptable, however, as the increase in frictional resistance is the most significant contributor to the overall penalty from hull roughness.

The core concept of this method, illustrated schematically in Fig. 3, is to determine the frictional resistance of the rough surface ($C_{Fs_{rough}}$) by finding the intersection of the ship's performance curve and a roughness-adjusted friction line. The key output is the net increase in the frictional resistance coefficient (ΔC_{Fs}), which is the difference between the frictional resistance of the rough hull and that of an equivalent smooth hull ($C_{Fs_{smooth}}$). as shown in Eq. (9). The final added resistance due to hull fouling ($\Delta R_{fouling}$) is then calculated by applying this net increase as described in Eq. (10). The detailed, iterative steps to determine these values are provided in the Supplementary material S1.

$$\Delta C_{Fs} = C_{Fs_{rough}} - C_{Fs_{smooth}} \tag{9}$$

$$\Delta R_{fouling} = \frac{1}{2}\rho V^2 S \Delta C_{Fs} \tag{10}$$

where ρ is the seawater density [kg/m^3], and S is the wetted surface area of the ship's hull [m^2].

2.4. Performance prediction module

2.4.1. Propulsive efficiency estimation

The total efficiency (η_T) of a ship's propulsion system can be expressed as a product of several efficiency coefficients as in Eq. (11)

$$\eta_T = \eta_H \times \eta_O \times \eta_R \times \eta_S \tag{11}$$

where η_H is the hull efficiency, η_O is the open water efficiency, η_R is the relative rotative efficiency, and η_S is the shaft efficiency

The hull efficiency (η_H) accounts for the hydrodynamic interaction between the hull and the propeller, which is calculated by Eq. (12). The thrust deduction factor and wake fraction in this equation are estimated using the empirical formulas within the Holtrop-Mennen method, which is the same methodology used for the calm water resistance estimation in Section 2.3.1. To estimate the open water efficiency (η_O) using only limited propeller information, the approximation formulas (Breslin and Andersen, 1994; Kristensen and Lützen, 2012) of Eqs. (13)–(15), which are based on Wageningen B-series propeller data (Van Lammeren et al., 1969) are applied. Furthermore, the relative rotative efficiency (η_R) and shaft efficiency (η_S) are assumed to be 1.0 and 0.98, respectively, which are typical values for conventional single-screw ships (Kristensen and Lützen, 2012).

$$\eta_H = \frac{1-t}{1-w} \tag{12}$$

$$\eta_O = \frac{2}{1+\sqrt{C_{Th}+1}} f(C_{Th}) \tag{13}$$

$$f(C_{Th}) = 0.81 - 0.014 C_{Th} \tag{14}$$

$$C_{Th} = \frac{8}{\pi} \frac{R_T}{\rho(1-t)\left((1-w)VD_p\right)^2} \tag{15}$$

where C_{Th} is thrust loading coefficient, t is thrust deduction factor, w is

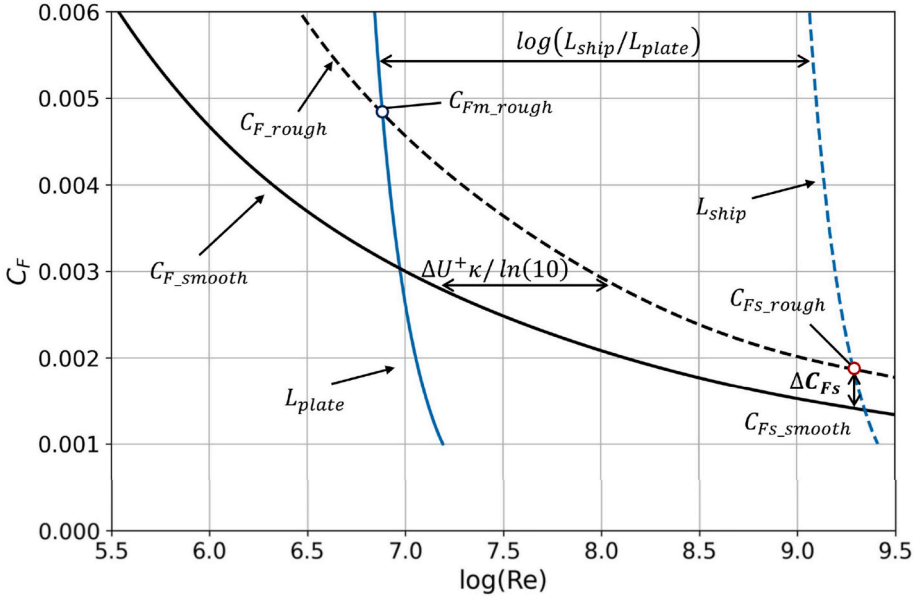

Fig. 3. Schematic diagram of Granville's similarity law scaling.

wake fraction, ρ is sea water density, and D_p is propeller diameter.

An increase in propeller surface roughness leads to higher frictional and form resistance of the propeller blade sections. Consequently, at the same rotational speed and advance velocity, the thrust coefficient (K_T) tends to decrease, while the torque coefficient (K_Q) tends to increase. The ITTC '78 Performance prediction method (ITTC, 2021) recommends a correction procedure to estimate this decrease in K_T and increase in K_Q due to propeller roughness, and subsequently to calculate a modified open water efficiency $\eta_O = J{\cdot}K_{TR}/(2\pi{\cdot}K_{QR})$ (here, K_{TR} and K_{QR} are the thrust and torque coefficients for the rough propeller, respectively, and J is the advance coefficient). This correction requires detailed propeller design information and an estimation of the changes in drag and lift coefficients resulting from the surface roughness.

While propeller fouling can contribute to overall performance degradation, there is a lack of reliable long-term fouling data for propellers that can be implemented in a simplified method. It is also recognized that hull fouling is related to propeller fouling and its associated increase in roughness, but quantifying the correlation between them is challenging. Given that the primary focus of this research is on analyzing the impact of hull fouling, the calculation of open water efficiency corrections due to changes in propeller roughness is omitted in the current model. Therefore, the open water efficiency is estimated by Eq. (13).

2.4.2. Power and fuel consumption calculation

The brake power (P_B) of the ship's main engine is calculated using the ship's total resistance (R_{Tw}) from Section 2.3 and the total efficiency (η_T) from Section 2.4.1, as shown in Eq. (16).

$$P_B = \frac{R_T \times V}{\eta_T} \tag{16}$$

The hourly fuel consumption of the ship ($FC(t)$) can be estimated as shown in Eq. (17), using the calculated main engine brake power ($P_B(t)$) and the specific fuel oil consumption (SFOC), which represents the fuel efficiency at the corresponding engine load. SFOC varies depending on the type of fuel oil, engine type, and engine load factor (MAN Diesel & Turbo, 2011). Furthermore, pollutant emissions from the ship due to fuel use ($EM(t)$) can be calculated as shown in Eq. (18) by multiplying the hourly fuel consumption ($FC(t)$) by the emission factor (EF) for each type of pollutant generated from the specific fuel and combustion process. In this study, the ship's SFOC and emission factors are determined with reference to data from the IMO Fourth GHG Study (Faber et al., 2020).

$$FC(t) = P_B(t) \times SFOC \tag{17}$$

$$EM(t) = FC(t) \times EF \tag{18}$$

2.4.3. Environmental performance indicator calculation

To evaluate the environmental performance of the vessel under different scenarios in a standardized manner, the Carbon Intensity Indicator (CII) was calculated according to the IMO guidelines (IMO, 2022). The attained annual CII is defined as the ratio of the total mass of CO_2 emitted to the total transport work in a given year and is calculated using the following Eq. (19).

$$attained\ CII = \frac{\sum FC_j \times C_{f_j}}{C \times D_t} \tag{19}$$

where FC_j is the total mass of consumed fuel oil of type j, C_{f_j} is the CO_2 conversion factor for fuel oil type j, C represents the ship's capacity, and D_t is the total distance travelled.

3. Case studies

This section details the simulation scenarios and conditions used to demonstrate the applicability of the proposed semi-empirical ship powering prediction model considering hull fouling in tropical waters and to analyze the impact of different operational and hull maintenance conditions on ship performance.

3.1. Simulation setup and conditions

To test and demonstrate the framework's capabilities in a relevant environment, a case study was designed for a container ship operating on a representative tropical sea route between Singapore and Semarang, Indonesia (see Table 3). This vessel is assumed to operate regularly on the route between Singapore and Semarang, Indonesia. One round trip is set to take a total of 7 days, with 2 days spent berthed at the ports of call (1 day each in Singapore and Semarang) and the remaining 5 days for sailing. The percentage of berthing time of the total voyage is approximately 28.6%. The operational speed is assumed to be maintained constantly at an average of 14.5 knots southbound and 10.5 knots northbound for each leg of the voyage, and the draught is assumed to be constant at 10.5 m. This operational profile for the vessel was established by referencing the average operational patterns of the ship navigating similar routes, and the detailed conditions are summarized in Table 4. For the fuel consumption and emission calculations specific to this case study, an average SFOC of 175 g/kWh and a CO_2 EF of 3.114 t-CO2/t-Fuel were applied, based on values from the IMO Fourth GHG Study (Faber et al., 2020).

To reflect the marine environmental conditions that affect added resistance during ship operation, this study utilized ERA5 reanalysis data provided by the European Centre for Medium-Range Weather Forecasts (ECMWF). Specifically, wind data (speed, direction) were sourced at a 1-h temporal and 0.25° × 0.25° spatial resolution, while wave data (significant wave height, peak period, mean wave direction) were sourced at a 1-h temporal and 0.5° × 0.5° spatial resolution. Considering the target vessel's operational schedule and its geographical position at each time point, these environmental variables were linearly interpolated from their respective native grids to the vessel's specific coordinates for each time-step. This interpolated time-series data was then used as the input for the resistance calculations. To calculate the added resistance in waves, the 2-parameter Pierson-Moskowitz wave spectrum was applied using the interpolated H_s and T_p values. Fig. 4 shows the yearly averaged environmental conditions for the target vessel's sailing region.

3.2. Scenarios

To quantitatively predict and comparatively analyze the impact of various operational conditions and hull maintenance strategies affecting ship performance using the proposed semi-empirical framework, a total of seven different simulation scenarios were established, as shown in Table 5. All scenarios were simulated for a total of three years of operation to analyze the long-term effects of biofouling and the effectiveness of different hull management strategies.

Scenario 1 assumes ideal conditions where the hull surface remains hydraulically smooth with no biofouling (berthing ratio of 28.6%). It serves as a theoretical benchmark for comparison with the results of other scenarios. Scenario 2 evaluates the impact of changes in the ship's

Table 3
Ship particulars.

Parameter	Value
Ship type	Container ship
Length between perpendiculars [m]	Abt. 165.0
Breadth [m]	Abt. 28.0
Design draught [m]	Abt. 10.5
Gross tonnage [tons]	Abt. 21,000
Deadweight tonnage [tons]	Abt. 26,000
Volume displacement [m3]	Abt. 35,000
TEU capacity [TEU]	Abt. 1800

Table 4
Ship operational profile.

Route	Berthing time percentage	Sailing speed	Sailing draught
Singapore-Semarang, Indonesia	28.6% (2 days berthing/5 days sailing)	Southbound: 14.5 knots/ Northbound: 10.5 knots	10.5 m

operational profile on fouling growth and ship performance. Here, Scenario 2a simulates a vessel with a typical antifouling coating operating according to the reference operational profile and subject to natural fouling progression without hull cleaning. This serves as a practical baseline for comparing the effectiveness of different coating types and maintenance strategies. Scenario 2b analyzes the impact of a 1.5-fold increase in berthing time (resulting in a berthing time percentage of 44.4%) while maintaining the same AFC coating and no cleaning conditions as Scenario 2a. Scenario 3 analyzes performance changes resulting from different hull surface conditions. Scenario 3a models a worst-case condition where the antifouling topcoat is assumed to be completely ineffective or absent, exposing the underlying anticorrosive layer to the marine environment. This acts as a control scenario to quantify the impact of unchecked biofouling. Scenario 3b, in contrast, evaluates a high-performance foul-release coating.

Finally, Scenario 4 reflects changes due to in-water hull cleaning (IWHC) strategies applied after fouling accumulation. The initial hull roughness condition applied after IWHC is set to a state of negligible wear, meaning the average hull roughness is restored to the initial coating condition. Scenario 4a represents a regular maintenance strategy where IWHC is performed at fixed 12-month intervals. Scenario 4b simulates a condition-based maintenance strategy where IWHC is performed when the additional brake power due to hull fouling increases by 8% or more, based on the upper bound of the 95% confidence interval.

4. Results and discussion

This section presents the results obtained from the proposed framework. First, the development and performance of the time-dependent fouling growth model, which is a key component of the framework, are presented. Subsequently, the complete framework is applied to various case studies to analyze the impact of biofouling and maintenance strategies on ship performance.

4.1. Fouling growth model development

Table 6 shows the model coefficient values and the goodness of fit of the model obtained by fitting Eq. (2). Fig. 5 provides a visual representation of the results of converting the field test data in Table 1 to the NSTM fouling rating scale, as well as the developed fouling growth model curves and their 95% confidence intervals for each coating type.

The R^2 value for the anticorrosive coating model is 0.5106, which is interpreted to be mainly due to the inherent heterogeneity of the data collected from different sources and conditions. The R^2 values for the antifouling and foul-release coating models are relatively low, at 0.3243 and 0.1397, respectively. In addition to the data heterogeneity, this is likely due to the superior antifouling effect of these coatings, which causes the FR_{NSTM} values to remain close to zero for long periods of time, resulting in a smaller variance in the observed fouling ratings. However, despite the low R^2 in the AFC/FRC cases, the Gaussian model was chosen for its empirical fit and ease of parameterization for early-stage fouling growth. Especially for data clustered near zero, the R^2 value may not be a reliable indicator of model fit. Rather, the RMSE (root mean square error) values presented in Table 6 indicate that the average prediction error corresponds to a relatively small difference in the actual fouling rating scale (e.g., initial slime formation or mild fouling levels),

Table 5
Definition of simulation scenarios. AC, Anticorrosive coating; AFC, Antifouling coating; FRC, Foul-release coating; IWHC, In-water hull cleaning.

No.	Scenario	Specific condition	Coating type	Berthing time (% of total)	Hull maintenance
1	Ideal condition	Hydraulically smooth hull	-	28.6%	No fouling growth applied
2	Operational profile change	(a) Reference operation	AFC	28.6%	No cleaning
		(b) Increased berthing time	AFC	44.4%	No cleaning
3	Coating type change	(a) Control coating (AC; surface without antifouling properties)	AC	28.6%	No cleaning
		(b) Foul-release coating	FRC	28.6%	No cleaning
4	IWHC strategy	(a) Regular IWHC on reference operation	AFC	28.6%	Every 12 months
		(b) Condition-based IWHC on reference operation	AFC	28.6%	$\Delta P_B \geq 8\%$

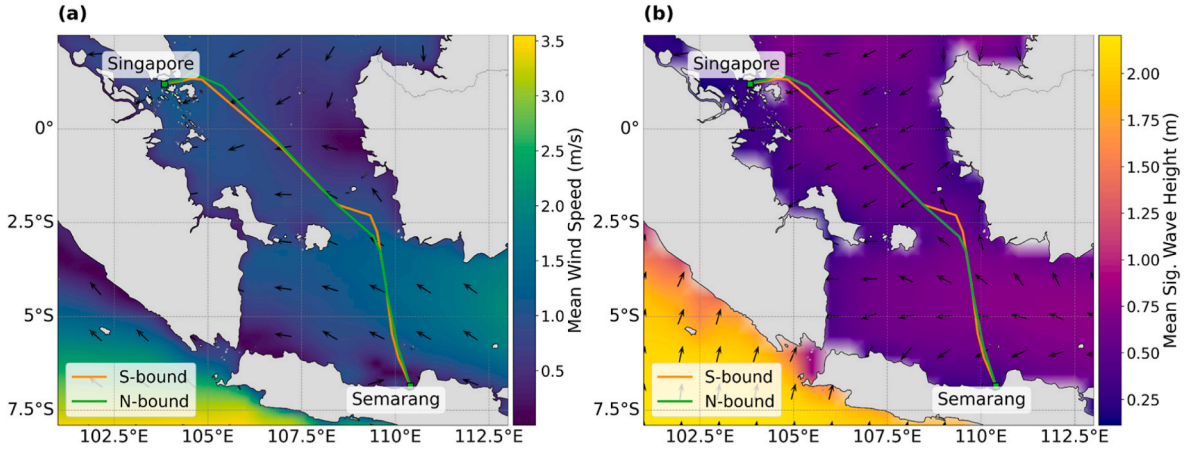

Fig. 4. Main shipping routes and annual average marine environmental conditions. (a) Mean wind speed and wind direction, and (b) Mean significant wave height and wave direction.

Table 6
The coefficients for the time-dependent fouling growth model in tropical waters.

Coating type	Model	Coefficient a	Coefficient b	Coefficient c	R^2 score	RMSE
Anticorrosive coating	Average	100	999.10	774.19	0.5106	10.79
	95CI upper		947.50	775.09	-	-
	95CI lower		1046.05	765.36	-	-
Antifouling coating	Average		1118.54	443.87	0.3243	2.30
	95CI upper		1258.97	559.01	-	-
	95CI lower		862.48	270.45	-	-
Foul-release coating	Average		2454.61	1678.56	0.1397	7.84
	95CI upper		2374.62	1730.52	-	-
	95CI lower		2495.14	1585.49	-	-

supporting the model's practical utility. As can be seen in Fig. 5, each coating type model reasonably represents the overall growth and accumulation trend of fouling over time in tropical waters. The pronounced scatter in Fig. 5 reflects substantial inter-study heterogeneity in site conditions, immersion depth, coating system, and experimental protocol. Therefore, the fitted curves should not be interpreted as deterministic predictions of local fouling evolution, but rather as smoothed coating-specific trend representations for comparative scenario simulations.

4.2. Baseline speed-power characteristics and hull fouling impact

In this section, the impact of different levels of hull fouling on the ship's speed-power characteristics under the average environmental conditions is quantitatively analyzed, and a fundamental application of this framework is demonstrated. Fig. 6 shows the required brake power versus ship speed for the target vessel at its design draught, based on the annual average wind and wave conditions defined in Section 3.1, with various hull roughness conditions defined by Schultz (2007) applied. The bottom black solid line represents the base speed-power curve for the ship operating under these average environmental conditions with a hydraulically smooth hull ($k_s = 0\mu m$), which represents the best possible performance under realistic environmental conditions. The remaining curves in Fig. 6 illustrate the total required brake power above this baseline, corresponding to conditions ranging from the initial application of a typical antifouling coating ($k_s = 30\mu m$) to different degrees of slime and calcareous fouling ($k_s = 0 - 10,000\mu m$).

It can be clearly observed that as hull roughness increases, the additional power demand due to fouling significantly increases across all speed ranges. For instance, at an operational speed of 15 knots, the smooth hull conditions necessitated roughly 5800 kW. If the hull surface was covered with light slime or experienced coating deterioration, the overall power consumption escalated to around 6400 kW, and further rose to around 11,000 kW in cases of heavy calcareous fouling. This indicated an incremental power demand of roughly 10% and 90% attributable to each of these fouling states in comparison to the hydraulically smooth hull. This analysis suggested that particularly severe fouling conditions could result in significant energy losses and potentially make normal operation of a ship impossible in certain speed ranges. This conceptual analysis quantitatively demonstrated the significant additional burden that increased hull roughness imposed on the ship's energy penalty, emphasizing the importance of effective hull condition management.

4.3. Voyage simulation & scenario analysis

This section presents the results of simulating the long-term performance changes for the different scenarios defined in Section 3.2 using the integrated framework proposed in Section 2. The three-year changes in hull surface condition for each scenario predicted by applying the fouling growth and roughness estimation module of the proposed framework are presented in Fig. 7(a), and the consequent impact of such roughness changes on the cumulative fuel consumption is shown in Fig. 7(b). Through this case study, the effects of different coating types (S2a, S3a, S3b), operational profiles (S2a, S2b), and maintenance strategies (S2a, S4a, S4b) on hull surface condition and fuel consumption can be compared. The 95% confidence intervals shown in Fig. 7 are mainly due to the uncertainty of the fouling growth model and the range of initial hull roughness settings, and they tend to be wider towards the longer-term predictions. Since the current framework has not yet been validated using independent full-scale ship performance data, the results of the scenarios discussed below should be interpreted as indicative of general trends observed under the assumed case study conditions.

As expected, the ideal case representing a hydraulically smooth hull condition without any hull roughness increase (S1) shows the lowest cumulative fuel consumption (Fig. 7(b)), which serves as a theoretical optimum case. For the baseline scenario 2a with antifouling coatings in this study, the hull roughness increased moderately and reached about 50 μm or more after 3 years, which led to a continuous increase in cumulative fuel consumption. On the other hand, scenario 3a with anticorrosive coating showed much faster increase in hull roughness than AFC, exceeding about 500 μm after 3 years, which resulted in the highest cumulative fuel consumption as shown in Fig. 7(b). This clearly illustrated the significant impact of the difference in antifouling efficacy of the coatings on hull roughness and highlighted the consequent energy penalty from the reduced operational efficiency of the ship. Meanwhile, scenario 3b with foul-release coating initially showed a very low k_s value, and then it gradually increased to show a slightly higher k_s value than scenario 2a in the third year. As a result, the cumulative fuel consumption over the total operating period was not significantly different from scenario 2a. However, the results for scenario S3b should be interpreted with caution. It should be noted that the fouling growth model for FRC is derived from static immersion tests, which do not fully capture the shear-induced fouling release mechanism that occurs during actual ship movement. This implies that the model likely underestimates the antifouling effectiveness of FRC systems under a ship's operating conditions. Consequently, the predicted k_s values for S3b are potentially overestimated, and better fouling release performance than predicted is expected at the vessel's actual operational speeds.

The impact of the operational profile is also clearly evident in Fig. 7. Scenario 2b with an increased berthing time (44.4%) showed a noticeably steeper k_s increase after about 300 days compared to the reference operational profile (S2a). This reflects the model's assumption (see Section 2.2) that increased berthing time accelerates fouling attachment and growth. Although increased hull roughness generally imposes a larger energy penalty for the ship, it can be seen in Fig. 7(b) that the cumulative fuel consumption for scenario 2b was significantly smaller than that of scenario 2a and other scenarios. This was because in scenario 2b, the ship spent more time in berth over the same three-year simulation period, which resulted in a shorter total sailing distance (or fewer sailing days) than the other scenarios. In other words, rather than indicating better energy efficiency, this could be interpreted as the vessel having accomplished fewer voyages and cargo transports within the same timeframe.

In Scenario 4, each IWHC strategy is subject to the logic of k_s value reset to a predefined $k_{s,initial}$ and subsequent k_s regrowth due to fouling as

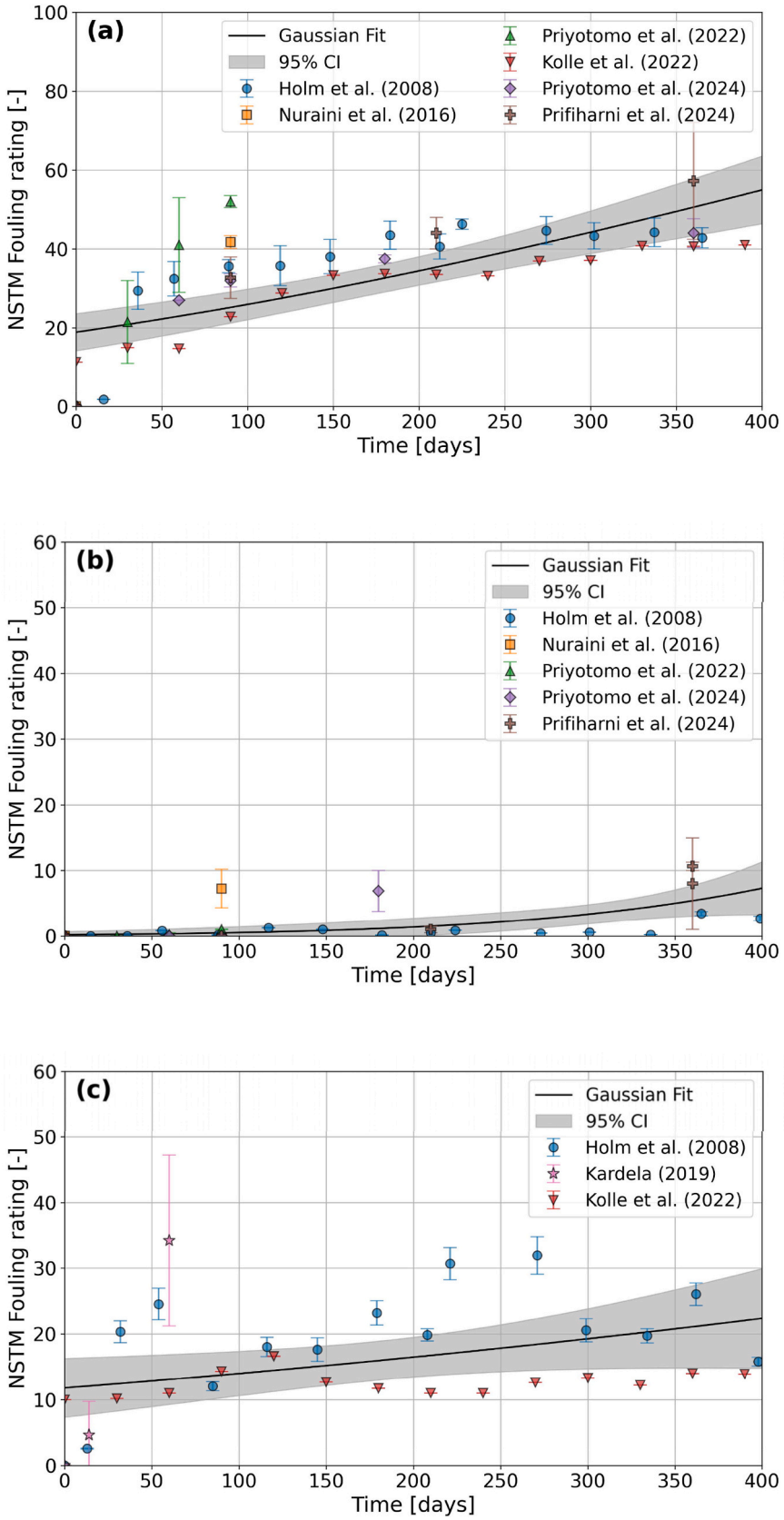

Fig. 5. Time-dependent fouling growth models developed in this study for (a) anticorrosive coating, (b) antifouling coating, and (c) foul-release coatings. The models are compared against the compiled field data from tropical waters used for fitting.

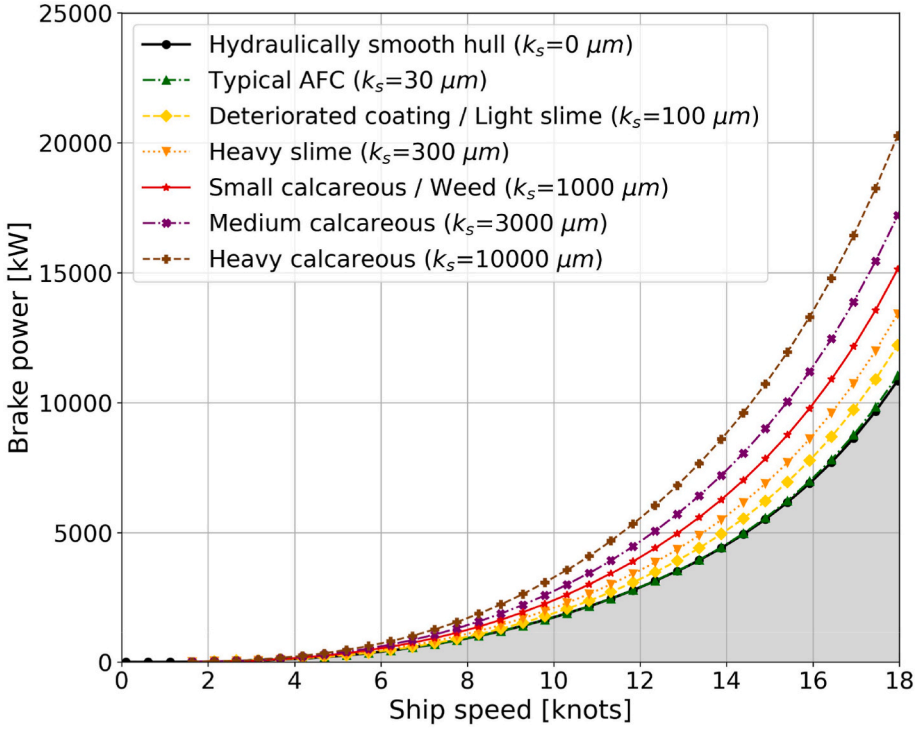

Fig. 6. Speed-power curves for the container ship at design load under different hull fouling conditions. The baseline curve illustrates the required brake power for a ship with a smooth hull under average environmental conditions.

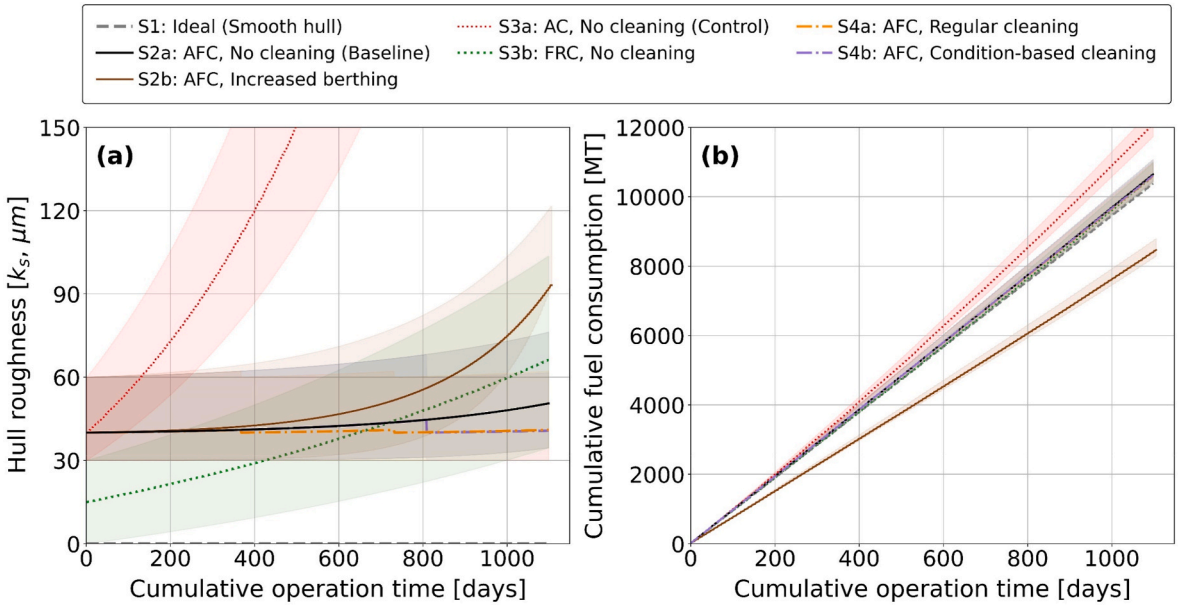

Fig. 7. (a) Change in hull roughness over cumulative operation time per hull maintenance scenario. Solid lines represent the mean simulation prediction for each scenario. The shaded area represents the predicted 95% confidence interval for k_s in each scenario, incorporating both the range of initial k_s values and the uncertainty of the fouling growth model. **(b)** Comparison of cumulative fuel consumption over cumulative operation time per hull maintenance scenario.

described in Section 2.2.3. As shown in Fig. 7(a), in scenario 4a, IWHC was applied every 12 months, which resulted in two cleaning events during the simulation period. In scenario 4b case, hull cleaning was performed once at around 800 days when the additional propulsive power due to fouling reached the predefined threshold of 8%. Fig. 7(b) showed that the fuel saving effect of such cleaning strategies assumed in this study was not as markedly pronounced compared to scenario 2a (no cleaning) as one might initially expect. This was likely due to a combination of factors that there were only one or two times of cleaning applied during the entire voyage, and the baseline scenario 2a already

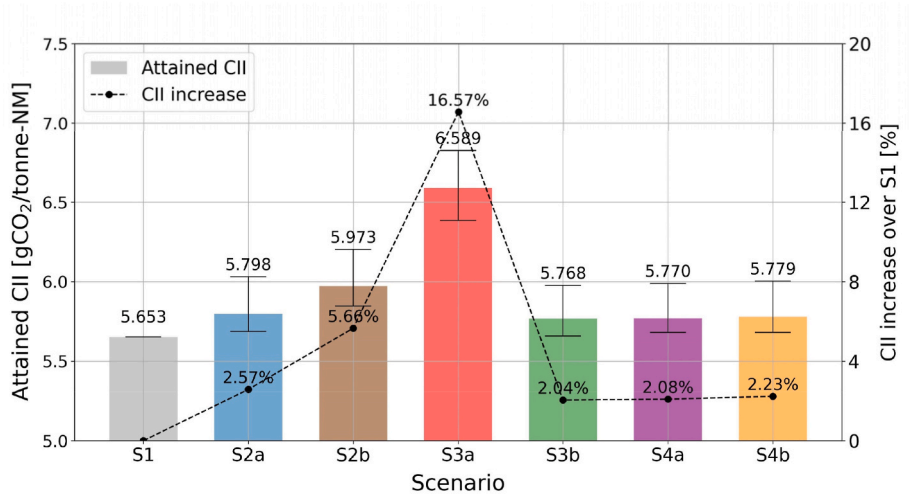

Fig. 8. Comparison of attained CII (bars) and relative percentage increase of CII to ideal case (S1) across simulation scenarios (connected points). The error bars represent the 95% confidence interval (CI) propagated from the uncertainty in the fouling growth model (95% CI from Table 6) and the range of initial hull roughness ($k_{s,init}$) settings (Table 2). Scenario labels follow Table 5: S1, ideal smooth hull; S2a/S2b, AFC with reference/increased berthing and no cleaning; S3a/S3b, AC control/FRC, both with no cleaning; S4a/S4b, AFC with regular/condition-based IWHC.

maintained a relatively moderate k_s progression under the specified operational scenario in this study. Thus, while cleaning provides benefits, its overall impact relative to an uncleaned AFC hull might be less dramatic if the fouling accumulation itself is not severe within the cleaning intervals or before the reactive threshold is met.

While it is based on a single vessel case, the results of this scenario analysis are noteworthy when compared to studies in other regions. The finding that cumulative idle time is a major contributor to fouling growth aligns with results from other research. However, the study by Kim et al. (2025) on RoPax vessels operating in the Baltic Sea also identified the regional salinity gradient as a key driver of fouling growth. In stable, highly saline tropical waters such as those in this study, this environmental variable is less pronounced, and the operational profile is likely to be a more dominant factor. Furthermore, while the biocide-free foul-release coatings are identified as the most cost-effective and sustainable option in the Baltic Sea study, the current study found that both biocide-free foul-release and biocidal antifouling coatings showed similarly high performance in terms of energy efficiency. Ultimately, these findings highlight that hull maintenance strategies must be tailored to the specific environmental pressures and operational profiles of a vessel's operating region.

To enable a standardized comparison of environmental performance across scenarios and to demonstrate the framework's utility for regulatory compliance decision-making, the CII was calculated for each case as described in Section 2.4.3. Fig. 8 presents the average attained annual CII for each scenario and its relative increase compared to the ideal case (S1). As the CII metric is based on the annual sailing distance and total CO_2 emissions (IMO, 2022), it allows for a robust quantitative comparison of transport efficiency across all scenarios, including those with varying operational profiles like S2b.

Within the mean scenario results, S3b (foul-release coating) and S4a (antifouling coating with regular hull cleaning) showed the lowest predicted CIIs of 5.768 $gCO_2/tonne-nm$ and 5.770 $gCO_2/tonne-nm$ among the non-ideal cases. However, the overlap of the propagated 95% confidence intervals indicates that these differences should not be interpreted as statistically distinct outcomes. This result is consistent with the overall fuel consumption trends observed in Fig. 7. On the other hand, scenario 2b with the longer berthing time at 44.4%, showed an increase in CII over ideal condition of about 5.66%, which is higher than the other scenarios. This indicates that despite lower total fuel consumption, the reduced total sailing distance can lead to a relatively unfavorable CII, an indicator of transport efficiency. The scenarios with in-water hull cleaning (S4a, S4b) resulted in CII values of around 5.770-5.779 $gCO_2/tonne-nm$, which showed a modest improvement in carbon intensity indicator compared to the 5.798 $gCO_2/tonne-nm$ of scenario 2a (baseline scenario without cleaning).

To understand the practical significance of these CII results, it is important to analyze them in the context of the vessel's operational profile and regulatory framework. The attained CII values for all scenarios in this study are significantly lower than the required CII thresholds applicable to container ships of equivalent capacity in 2025, which is enough to achieve a major superior (A rating). This highly favorable rating is due to the fact that slow-steaming profiles (10.5-14.5 knots) for container ships like the one in the case study have significantly lower annual CO_2 emissions than operations closer to design speed.

However, the key insight lies in the relative differences between the scenarios. Notably, the CII gap between the worst-case control scenario (S3a) and a well-maintained scenario (S4a) was approximately 14%. This margin is substantial enough to potentially shift a vessel's rating across different bands under more demanding, real-world operational conditions. Given that CII regulations will become increasingly stringent towards 2030, this finding highlights that proactive hull management is essential for maintaining and improving regulatory compliance.

This essential role in compliance underscores the broader strategic importance of hull maintenance as a key decarbonization lever. While the maritime industry pursues long-term solutions such as alternative fuels and wind-assisted propulsion, which require significant capital investment, optimizing hull condition represents an immediate and highly cost-effective low-hanging fruit. It is a foundational strategy that can be implemented today across the existing ship fleet and can be combined with other energy-saving measures to maximize emissions reduction.

These CII analysis results show that the proposed framework can extend beyond simple fuel consumption predictions to quantitatively compare and analyze the effectiveness of different hull maintenance options, such as coating selection, optimizing the frequency and timing of hull cleaning, and adjusting operational schedules, in response to environmental regulations. Therefore, it can make informed decisions for the operator to satisfy regulatory requirements by proactively evaluating CII changes under different conditions.

5. Conclusions

This study proposed a novel semi-empirical framework to quantitatively predict the impact of biofouling on the performance of ships operating in tropical waters and demonstrated its applicability. For this purpose, an empirical fouling growth model was established based on actual field test data from tropical waters to predict the time-dependent changes in equivalent sand-grain roughness for various antifouling systems. This model was then integrated with hull maintenance activities and the subsequent fouling regrowth processes. Furthermore, it was coupled with a ship resistance and energy consumption estimation module to comprehensively simulate long-term changes in ship powering performance and environmental indicator due to fouling accumulation and management activities.

Through case studies based on various scenarios, the immediate impact of fouling conditions on the ship's speed-power performance was quantified. Furthermore, the long-term effects of diverse variables such as coating type, operational profile, and in-water hull cleaning strategies on hull roughness and cumulative fuel consumption over a three-year period were comparatively analyzed. The results showed that among the scenarios analyzed in this study, the scenarios with foul-release coating or antifouling coating with regular hull cleaning can contribute the most to fuel/GHG efficiency improvement. Meanwhile, increased berthing time was identified as a main contributor to fuel efficiency degradation by accelerating fouling growth. The study also quantified the severe penalty in terms of both hull roughness and fuel consumption associated with coating failure or the absence of an effective antifouling system by modeling the control scenario with an unprotected anticorrosive surface. This reinforces the economic and environmental necessity of proactive hull maintenance. These results demonstrate that the proposed framework is useful for predicting and evaluating performance variations due to changes in actual ship operating conditions and management strategies.

The framework developed in this study provides a practical decision-support tool for operators of ships that frequently sail or spend time at berth in tropical waters. It enables a more accurate prediction of changes in fuel consumption and GHG emissions, which allows a proactive evaluation of various hull management strategies. This is expected to enhance ship energy efficiency, decrease operating expenses, and improve the sustainability of the shipping sector.

While the proposed framework offers a practical and computationally efficient approach to predict ship performance under tropical fouling conditions, it is important to acknowledge areas for further refinement. Limitations exist primarily in the fouling growth modeling and hydrodynamic resistance calculations. The current fouling growth model employs a generalized trend for tropical waters, an approach adopted to maintain robustness given the heterogeneous field data from differing experimental protocols. Additionally, it utilizes static immersion test data for foul-release coatings, which may underestimate FRC performance by neglecting dynamic self-cleaning mechanisms. In terms of resistance calculation, the framework estimates hull fouling effects by converting biofouling states to an averaged equivalent roughness and applying Granville's scaling. This approach primarily accounts for frictional resistance changes, simplifying complex effects like discrete form drag from hard fouling, and does not yet incorporate the impact of propeller roughness.

Since the compiled tropical datasets are heterogeneous and independent full-scale ship performance data were not available for validation, the quantitative results reported here should be interpreted as indicative comparative trends under the assumed case-study conditions. A key priority for future work is therefore to compare alternative fouling-growth formulations using larger standardized tropical datasets and to validate the full modelling chain against full-scale operational data. Building upon the current framework, subsequent application studies should focus on more sophisticated modeling of hull maintenance, which explores the optimization of cleaning based on fouling intensity and assesses the economic and environmental trade-offs of different cleaning qualities. Validating the framework against actual ship operational data will also be a crucial next step to further solidify its real-world applicability.

CRediT authorship contribution statement

Youngrong Kim: Writing – review & editing, Writing – original draft, Visualization, Software, Project administration, Investigation, Funding acquisition, Formal analysis, Conceptualization. **Shukui Liu:** Writing – review & editing, Methodology, Conceptualization. **Maria Lagerström:** Writing – review & editing, Methodology, Conceptualization. **Lena Granhag:** Writing – review & editing, Methodology, Conceptualization. **Erik Ytreberg:** Writing – review & editing, Methodology, Conceptualization.

Declaration of competing interest

The authors declare that they have no known competing financial interests or personal relationships that could have appeared to influence the work reported in this paper.

Acknowledgements

This work is funded by the Nanyang Technological University Start-up Grant (NTU-SUG).

Appendix A. Supplementary data

Supplementary data to this article can be found online at https://doi.org/10.1016/j.oceaneng.2026.125590.

Data availability

Data will be made available on request.

References

Atlar, M., Yeginbayeva, I., Turkmen, S., Demirel, Y., Carchen, A., Marino, A., Williams, D., 2018. A rational approach to predicting the effect of fouling control systems on "In-Service" ship performance. GMO Journal Of Ship And Marine Technology 24 (213), 5–36.

Bakka, H., Rognebakke, H., Glad, I., Haff, I.H., Vanem, E., 2022. Estimating the effect of biofouling on ship shaft power based on sensor measurements. Ship Technol. Res. 1–13. https://doi.org/10.1080/09377255.2022.2159108.

Blendermann, W., 1994. Parameter identification of wind loads on ships. J. Wind Eng. Ind. Aerod. 51 (3), 339–351. https://doi.org/10.1016/0167-6105(94)90067-1.

Bouman, E.A., Lindstad, E., Rialland, A.I., Strømman, A.H., 2017. State-of-the-art technologies, measures, and potential for reducing GHG emissions from shipping – a review. Transport. Res. Transport Environ. 52, 408–421. https://doi.org/10.1016/j.trd.2017.03.022.

Breslin, J.P., Andersen, P., 1994. Hydrodynamics of Ship Propellers (No. 3). Cambridge University Press.

Demirel, Y.K., Turan, O., Incecik, A., 2017. Predicting the effect of biofouling on ship resistance using CFD. Appl. Ocean Res. 62, 100–118. https://doi.org/10.1016/j.apor.2016.12.003.

Faber, J., Hanayama, S., Zhang, S., Pereda, P., Comer, B., Hauerhof, E., S, T., van der L, W.S., Z, Y., K, H., Xing, H., 2020. Fourth Imo Ghg Study. London, UK.

Farkas, A., Degiuli, N., Martić, I., Vujanović, M., 2021. Greenhouse gas emissions reduction potential by using antifouling coatings in a maritime transport industry. J. Clean. Prod. 295, 126428. https://doi.org/10.1016/j.jclepro.2021.126428.

Fujiwara, T., 2006. A new estimation method of wind forces and moments acting on ships on the basis of physical components models. J. Jpn. Soc. Nav. Archit. Ocean Eng. 2, 243–255. https://doi.org/10.2534/jjasnaoe.2.243.

Granville, P.S., 1958. The frictional resistance and turbulent boundary layer of rough surfaces. J. Ship Res. 2 (4), 52–74. https://doi.org/10.5957/jsr.1958.2.4.52.

Guo, B., Gupta, P., Steen, S., Tvete, H.A., 2023. Evaluating vessel technical performance index using physics-based and data-driven approach. Ocean. Eng. 286 (P2), 115402. https://doi.org/10.1016/j.oceaneng.2023.115402.

Holm, E.R., Wendt, D.E., Brewer, L., Connolly, J., Kowalke, G., Swain, G., Connelly, P., Kavanagh, C., Hadfield, M.G., Huggett, M., Nedved, B.T., 2008. Characterization of Fouling at Field Test Sites of the ONR Biofouling Program : Background Information and Results for 2006-2007. Bethesda, Md: Naval Surface Warfare Center Carderock Div Survivability Structures and Materials Directorate.

Holtrop, J., 1984. A statistical re-analysis of resistance and propulsion data. Int. Shipbuild. Prog. 31 (363), 272–276.
Holtrop, J., Mennen, G.G.J., 1982. An approximate power prediction method. Int. Shipbuild. Prog. 29 (335), 166–170. https://doi.org/10.3233/ISP-1982-2933501.
IMO, 2022. 2022 guidelines on operational carbon intensity indicators and the calculation methods (CII guidelines, G1). In Resolution MEPC 78/17/Add. 1. MEPC 352 (78). International Maritime Organization London, UK. https://wwwcdn.imo.org/localresources/en/KnowledgeCentre/IndexofIMOResolutions/MEPCDocuments/MEPC.352(78).pdf.
IMO, 2023. 2023 IMO strategy on reduction of GHG emissions from ships. Resolution MEPC 377 (80). International Maritime Organization (IMO). https://wwwcdn.imo.org/localresources/en/MediaCentre/PressBriefings/Documents/Resolution MEPC.377(80).pdf.
IPCC, 2022. Climate change 2022: mitigation of climate change. Contribution of Working Group III To the Sixth Assessment Report of the Intergovernmental Panel on Climate Change. https://doi.org/10.1017/9781009157926.
ITTC, 2021. ITTC - recommended procedures and guidelines performance prediction method. Resistance and Propulsion Committee of the 29th ITTC.
ITTC, 2022. ITTC – Recommended procedures and guidelines. Preparation, conduct and analysis of speed/power trials. Quality Systems Group of the 30th ITTC.
Kardela, J.H., 2019. *Investigation of (Super)Hydrophilic Coatings for Marine Antifouling Applications* (Issue September). Newcastle University.
Kim, Y., Lagerström, M., Granhag, L., Ytreberg, E., 2025. Sustainable hull maintenance strategies in Baltic sea region through case studies of RoPax vessels. Mar. Pollut. Bull. 211. https://doi.org/10.1016/j.marpolbul.2024.117453.
Kim, Y., Steen, S., Kramel, D., Muri, H., Strømman, A.H., 2023. Modelling of ship resistance and power consumption for the global fleet: the MariTEAM model. Ocean. Eng. 281, 114758. https://doi.org/10.1016/j.oceaneng.2023.114758.
Kolle, S., Ahanotu, O., Meeks, A., Stafslien, S., Kreder, M., Vanderwal, L., Cohen, L., Waltz, G., Lim, C.S., Slocum, D., Greene, E.M., Hunsucker, K., Swain, G., Wendt, D., Teo, S.L.M., Aizenberg, J., 2022. On the mechanism of marine fouling-prevention performance of oil-containing silicone elastomers. Sci. Rep. 12 (1), 11799. https://doi.org/10.1038/s41598-022-15553-4.
Kristensen, H.O., Lützen, M., 2012. Prediction of resistance and propulsion power of ships. Clean Shipping Currents 1 (6), 1–52.
Kytariolou, A., Themelis, N., 2023. Optimized route planning under the effect of hull and propeller fouling and considering ocean currents. J. Mar. Sci. Eng. 11 (4), 828. https://doi.org/10.3390/jmse11040828.
Laurie, A., Anderlini, E., Dietz, J., Thomas, G., 2021. Machine learning for shaft power prediction and analysis of fouling related performance deterioration. Ocean. Eng. 234, 108886. https://doi.org/10.1016/j.oceaneng.2021.108886.
Leer-Andersen, M., 2018. Slutrapport För "Ytfriktionsdatabas För Maritima Sektorn" [RE40147243-02-00-A]. Gothenburg.
Lin, S., Bi, H., Weinell, C.E., Azizaddini, S., Dam-johansen, K., 2023. Systematic cleaning and evaluation of exposed fouling control coating systems using a novel laboratory scale automated underwater cleaning system. Prog. Org. Coating 182, 107712. https://doi.org/10.1016/j.porgcoat.2023.107712.
Liu, S., Kee, Y.H., Shang, B., Papanikolaou, A., 2023. Assessment of the economic, environmental and safety impact of biofouling on a ship's hull and propeller. Ocean. Eng. 285 (P2), 115481. https://doi.org/10.1016/j.oceaneng.2023.115481.
Liu, S., Papanikolaou, A., 2020. Regression analysis of experimental data for added resistance in waves of arbitrary heading and development of a semi-empirical formula. Ocean. Eng. 206, 107357. https://doi.org/10.1016/j.oceaneng.2020.107357.
Madin, J., Chong, V.C., Basri, B., 2009. Development and short-term dynamics of macrofouling assemblages on fish-cage nettings in a tropical estuary. Estuar. Coast Shelf Sci. 83 (1), 19–29. https://doi.org/10.1016/j.ecss.2009.03.012.
MAN Diesel & Turbo, 2011. Basic principles of ship propulsion. MAN Diesel & Turbo, Copenhagen, Denmark. http://www.mandieselturbo.com/files/news/filesof5405/5510_004_02low.pdf.
Martić, I., Degiuli, N., Majetić, D., Farkas, A., 2021. Artificial neural network model for the evaluation of added resistance of container ships in head waves. J. Mar. Sci. Eng. 9 (8). https://doi.org/10.3390/jmse9080826.
Nuraini, L., Prifiharni, S., Priyotomo, G., 2016. The corrosivity and performance evaluation of antifouling paint exposed in seawater Muara Baru port, Jakarta. J. Phys. Conf. 817 (1), 012068. https://doi.org/10.1088/1742-6596/755/1/011001.
Oliveira, D.R., Granhag, L., 2020. Ship hull in-water cleaning and its effects on fouling-control coatings. Biofouling 36 (3), 332–350. https://doi.org/10.1080/08927014.2020.1762079.
Oliveira, D.R., Lagerström, M., Granhag, L., Werner, S., Larsson, A.I., Ytreberg, E., 2022. A novel tool for cost and emission reduction related to ship underwater hull maintenance. J. Clean. Prod. 356, 131882. https://doi.org/10.1016/j.jclepro.2022.131882.
Ozyurt, R., Uzun, D., Terzi, Y., Şaffak, S., Atlar, M., Turan, O., 2023. A simple antifouling coating selection exhibits notable benefits for industrial fishing vessels. Ocean. Eng. 288. https://doi.org/10.1016/j.oceaneng.2023.115955.
Prifiharni, S., Nuraini, L., Priyotomo, G., Triwardono, J., Sundjono, Gunawan, H., Mudaryoto, J.W., 2024. The investigation of antifouling paint efficacy after long exposure in the Gulf of Benoa, Indonesia. In: AIP Conference Proceedings, vol. 2382, 060004. https://doi.org/10.1063/5.0061202.
Priyotomo, G., Prifiharni, S., Nikitasari, A., Musabikha, S., Kusumastuti, R., Nuraini, L., Triwardono, J., Nugraha, H., Prasetyo, A.B., Julistiono, H., 2024. Investigation of antifouling paints for vessel in tropical seawater of North Jakarta in Indonesia. Int. J. Eng. Trans. A: Basics 37 (1), 167–177. https://doi.org/10.5829/ije.2024.37.01a.15.
Priyotomo, G., Prifiharni, S., Nuraini, L., Royani, A., Sundjono, Gunawan, H., 2022. The performance of antifouling paint for prolonged exposure in Madura strait, East java province, Indonesia. Int. J. Adv. Sci. Eng. Inf. Technol. 12 (2), 732–737. https://doi.org/10.18517/ijaseit.12.2.10253.
Satheesh, S., Ba-Akdah, M.A., Al-Sofyani, A.A., 2016. Natural antifouling compound production by microbes associated with marine macroorganisms — a review. Electron. J. Biotechnol. 21, 26–35. https://doi.org/10.1016/j.ejbt.2016.02.002.
Schultz, M.P., 2007. Effects of coating roughness and biofouling on ship resistance and powering. Biofouling 23 (5), 331–341. https://doi.org/10.1080/08927010701461974.
Shaw, H.J., Lin, C.K., 2021. Marine big data analysis of ships for the energy efficiency changes of the hull and maintenance evaluation based on the ISO 19030 standard. Ocean. Eng. 232 (3), 108953. https://doi.org/10.1016/j.oceaneng.2021.108953.
Song, S., Dai, S., Demirel, Y.K., Atlar, M., Day, S., Turan, O., 2021. Experimental and theoretical study of the effect of hull roughness on ship resistance. J. Ship Res. 65 (1), 62–71. https://doi.org/10.5957/JOSR.07190040.
Song, S., Demirel, Y.K., Atlar, M., 2019. An investigation into the effect of biofouling on the ship hydrodynamic characteristics using CFD. Ocean. Eng. 175, 122–137. https://doi.org/10.1016/j.oceaneng.2019.01.056.
Thomas, D., Surendran, S., Vasa, N.J., 2021. A simplified approach for voyage analysis of fouled hull in a tropical marine environment. Ships Offshore Struct. 16 (7), 762–772. https://doi.org/10.1080/17445302.2020.1781745.
Townsin, R.L., 2003. The ship hull fouling penalty. Biofouling 19 (S1), 9–15. https://doi.org/10.1080/0892701031000088535.
UN, 2021. Review of Maritime Transport. UNCTAD. https://unctad.org/system/files/official-document/rmt2021_en_0.pdf.
US Navy, 2006. Waterborne Underwater Hull Cleaning of Navy Ships. Naval Ships' Technical Manuals.
Uzun, D., Demirel, Y.K., Coraddu, A., Turan, O., 2019. Time-dependent biofouling growth model for predicting the effects of biofouling on ship resistance and powering. Ocean. Eng. 191, 106432. https://doi.org/10.1016/j.oceaneng.2019.106432.
Uzun, D., Ozyurt, R., Demirel, Y.K., Turan, O., 2020. Does the barnacle settlement pattern affect ship resistance and powering? Appl. Ocean Res. 95, 102020. https://doi.org/10.1016/j.apor.2019.102020.
Uzun, D., Zhang, Y., Demirel, Y.K., Turan, O., 2017. Experimental determination of added resistance due to barnacle fouling on ships by using 3D printed barnacles. The 5th International Conference on Advanced Model Measurement Technology for the Maritime Industry (AMT'17), pp. 262–277.
Van Lammeren, W.P.A., van Manen, J.V., Oosterveld, M.W.C., 1969. The Wageningen B-screw series. Transactions SNAME 77, 269–317.
Wang, J., Bielicki, S., Kluwe, F., Orihara, H., Xin, G., Kume, K., Oh, S., Liu, S., Feng, P., 2021. Validation study on a new semi-empirical method for the prediction of added resistance in waves of arbitrary heading in analyzing ship speed trial results. Ocean. Eng. 240, 109959. https://doi.org/10.1016/j.oceaneng.2021.109959.
Yeginbayeva, I.A., Atlar, M., 2018. An experimental investigation into the surface and hydrodynamic characteristics of marine coatings with mimicked hull roughness ranges. Biofouling 34 (9), 1001–1019. https://doi.org/10.1080/08927014.2018.1529760.